Ukrainian Journal of Physical Optics
ISSUE 4
2024

A THREE-DIMENSIONAL FLOW FIELD MEASUREMENT METHOD BASED ON LIGHT FIELD PARTICLE STREAK VELOCIMETRY

MIAO YANG[1,2]

[1]School of Energy and Power Engineering, University of Shanghai for Science and Technology, Shanghai 200093, China
[2]Shanghai Key Laboratory of Multiphase Flow and Heat Transfer in Power Engineering, Shanghai 200093, China

Received: 05.07.2024

Abstract. Light field cameras can obtain 3D spatial information about objects by acquiring a single image, demonstrating that light field imaging technology does not require complex light path arrangements. Owing to this capability, light field cameras have recently attracted attention from various fields. Besides, particle streak velocimetry (PSV) is a non-contact image-based flow field measurement technique widely used in optical and image processing technology. It has obvious advantages in measuring high-speed flow fields. Hence, this paper combines light field imaging technology with PSV technology and introduces a new 3D velocity measurement system that exploits the advantages of both technologies to measure flow fields with narrow windows, fast flow rates, and difficult-to-arrange measurement equipment. The system developed constructs a three-dimensional flow field measurement method based on light field PSV, which is unique as no relevant research on the PSV 3D velocity measurement utilizes light field imaging. Specifically, the motion streak of a 5 μm point light source moving at different speeds was captured using a light field camera, and its 3D velocity field was verified and calculated using a computing system. The results demonstrated that the 3D flow field measurement method based on light field PSV can successfully measure 3D flow fields.

Keywords: light field imaging, 3D measurement, particle streak velocimetry
UDC: 535.2, 681.7
DOI: 10.3116/16091833/Ukr.J.Phys.Opt.2024.04038

1. Introduction.

Developing effective flow field measurement techniques is significant in solving complex problems in flow fields. Simplification and improving the effectiveness of flow field measurement technology should start with the hardware equipment and measurement methods used. Recently, light field cameras have rapidly advanced and gained significant research attention due to their capability to obtain 3D spatial information on objects in a single shot [1]. Such cameras can greatly simplify experimental operations, especially in measuring 3D flow fields with fewer or narrow optical windows.

In 1936, Gershun introduced the light field concept [2], and in 1991, Adelson et al. proposed a 7D all-optical function to characterize optical field information [3]. Due to the complexity of all-optical tasks that are not easy to visualize and calculate, in 1995, McMillan and Bishop et al. reduced the 7D all-optical function to a 5D function. They developed an image rendering technique based on the 5D function [4]. In 1996, Levoy and Hanrahan parameterized the light field with two parallel planes, thereby reducing the all-optical function to a 4D light field function $L(u, v, s, t)$. They also developed an image rendering method based on the 4D light field function [5]. Collecting the light field of a certain scene in space and then using mathematical methods of data processing to present the information of

the scene in 3D is called light field imaging technology [6]. The methods to collect the light field include a single camera, multi-camera array, and microlens array. Adelson designed an all-optical camera in 1992, but the light field images obtained exhibited severe vignetting due to the introduction of a relay lens during the design process [7]. In 2005, Ng et al. removed the relay lens and simplified the design of all-optical cameras, but the spatial resolution of this all-optical camera was lower [8]. In response to this issue, in 2008, Lumsdaine and Georgiev proposed a focused light field camera [9], which first images a certain plane in the object space through the primary lens on a virtual image plane at a certain distance behind the primary lens, and then the virtual image plane is re-imaged on the CCD detector plane through a microlens. This secondary imaging method has higher spatial resolution than all-optical cameras. In 2019, Thurow assembled a focused light field camera to measure flow velocity fields and diagnose combustion [10]. Broxton et al. developed light field microscopy imaging technology and built a cage-type light field camera for the first time [11]. Moreover, a tomographic particle image velocimetry (PIV) technology was first proposed based on light field cameras, i.e., light field tomography PIV [12-14], and a 3D velocity field was measured. Afterward, Thurow extensively investigated optical field PIV and applied it to velocity field measurements in actual flow fields, achieving significant progress [15-18]. However, light field PIV has many problems, such as the time-consuming weight matrix calculation, the necessity of the large storage capacity, the time-consuming tomographic reconstruction, and the stretching effect on the reconstructed particles in the depth direction. Therefore, researchers have gradually shifted toward combining light fields with particle-tracking velocimetry (PTV). Current 3D PTV technologies mainly include stereoscopic particle tracking velocimetry (SPTV) [19], defocusing digital particle tracking velocimetry (DDPTV) [20], Scanning particle tracking velocimetry (SSPTV) [21], and micro holographic particle tracking velocimetry (MHPTV) [22]. However, 3D PTV has limitations that need to be overcome: the experimental equipment layout is complex and expensive, and the processing algorithm is complex. Therefore, particle streak velocimetry (PSV) has received widespread attention as an image-based flow velocity measurement technique [23]. Compared to traditional flow field measurement techniques, it has the same advantages as PIV [24], i.e., non-contact full-field measurement and higher accuracy. However, compared to PIV technology, PSV requires lower hardware equipment: the camera and light source are not strictly synchronized, and high-power pulse lasers are unnecessary. This technology can also be considered a derivative of PTV [25]. Still, compared to PTV, PSV does not require a high frame rate image acquisition system and does not require matching between adjacent frames, avoiding algorithm complexity.

This article is based on the theoretical model of light field imaging combined with PSV velocity measurement technology. Specifically, the development of a 3D PSV flow field measurement method successfully applied to the 3D velocity field measurement experiment based on light field imaging is presented in this article. In the experiment, a point light source with a diameter of 5 μm was placed on an inclined orbit to simulate the 3D motion of tracer particles in flow field measurements. Using a long exposure lighting method, a light field camera captures the motion trajectories of the point light source moving at different speeds. A PSV 3D flow field measurement algorithm based on light field imaging is constructed to obtain the motion trajectories of the point light source at different speeds for verification and

calculation. The results demonstrate that the 3D velocity field measurement method based on light field PSV can be successfully applied.

2. Measuring principle

2.1. Principle of optical field refocusing.

The light field can be parameterized using light rays intersecting with two parallel planes [5]. The total energy $I(x,y)$ received by point (x,y) from the beam $L(u,v,x,y)$ is formulated as follows:

$$I(x,y)=\iint L(u,v,x,y)dudv\,. \tag{1}$$

Fig. 1 illustrates the refocusing principle diagram of a simplified two-dimensional light field. In this diagram, the virtual image point O_L is imaged on the sensor through a microlens as O_m, and O_r is the point of O_m after refocusing. A red arrow represents the beam L, U is the microlens plane, X is the imaging detector plane, X' is the refocusing plane, and l' is the distance between U and X'. Additionally, $l'=\alpha_{opt}l$, where α_{opt} is the refocusing coefficient. After a series of mathematical derivations, refocusing is mathematically formulated as follows:

$$I(x',y')=\iint L\left(u,v,\frac{1}{\alpha_{opt}}x'+\left(1-\frac{1}{\alpha_{opt}}\right)u,\frac{1}{\alpha_{opt}}y'+\left(1-\frac{1}{\alpha_{opt}}\right)v\right)dudv\,. \tag{2}$$

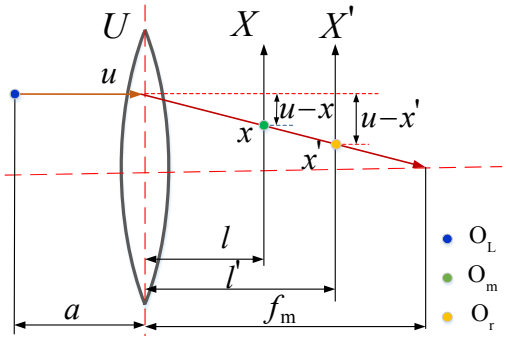

Fig. 1. Principle diagram of optical field refocusing.

2.2. Principle of depth measurement.

This article introduces the principle of depth measurement using the Kepler-type light field camera as an example. It should be noted that this principle also applies to the Galileo-type light field camera. Fig. 2 depicts the principle diagram of light transmission in a Kepler-type light field camera, where the object point O is imaged as the image point O_L through the primary lens. After passing through the microlens, O_L is imaged as O_m on the sensor, and O_r is the point of O_m after refocusing.

By combining the Gaussian imaging formula, it can be inferred that:

$$d=\left\{f_L^{-1}-\left[B_L-\left(f_m^{-1}-\left(\alpha_{opt}l\right)^{-1}\right)^{-1}\right]^{-1}\right\}^{-1}-a_0 \tag{3}$$

where f_L, f_m, B_L, α_0, and l are fixed parameters of the optical field imaging system. When the parameters of the camera and lens are determined, d has a unique correspondence with α_{opt} and d decreases as α_{opt} increases.

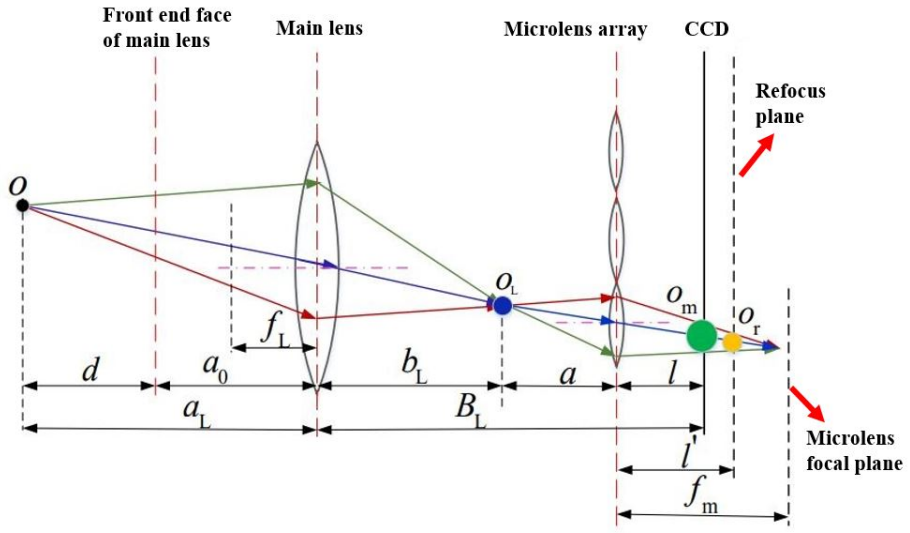

Fig. 2. Ray transmission diagram of a Kepler field camera.

2.3. Principle of 3D PSV of the light field.

The light field's 3D PSV velocity measurement technology mainly includes depth measurement and streak recognition. With the help of this technology, it first obtains a depth map by processing a 4D light field image, then obtains the image's 2D information through the all-focus map, determines the 3D on streak information, and combines the exposure time to obtain the speed. Fig. 3 presents the corresponding flowchart. Before measuring the flow field, it is mandatory to calibrate the center, depth, equivalent internal reference distortion coefficient, and magnification of the microlens of the light field camera.

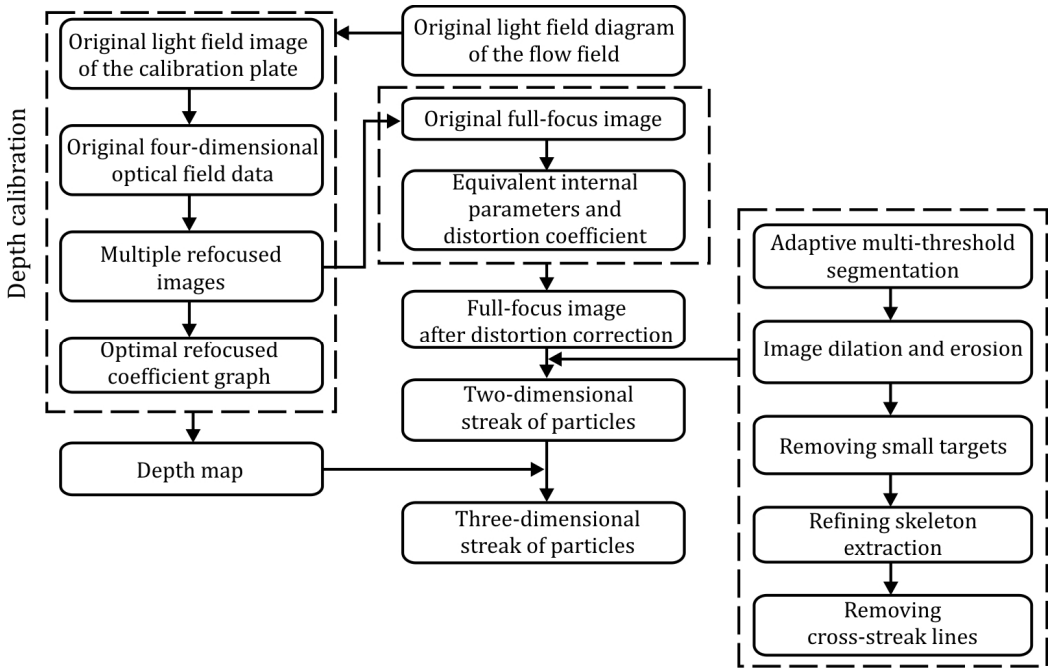

Fig. 3. Flowchart of the optical field PSV velocity measurement technology.

When measuring the flow field, the original light field image of the flow field is refocused multiple times. The optimal refocusing coefficient map and all-focus map of the flow field map are obtained based on the principle of maximum clarity. Combined with the depth calibration curve, the depth map of the flow field is obtained. The all-focus image of the flow field is corrected based on the calibrated equivalent intrinsic distortion coefficient. Then, the distortion-corrected image of the all-focus flow field is corrected to obtain the 2D streak positions of particles in the flow field. This preprocessing strategy is illustrated in Fig. 3, which mainly includes adaptive multi-threshold segmentation, image dilation and erosion, removing small targets, refining skeleton extraction, and removing cross-streak lines. After image preprocessing, there are multiple particle streaks with one-pixel width that do not intersect, and the coordinates of all points on each streak are known. Then, by indexing the depth of each point in the streak from the depth map, the 3D motion streak of the particles is obtained. Combined with the previously calibrated magnification, the 3D streak of the particles in the actual space is obtained, which is used to obtain the velocity based on the corresponding exposure time.

3. Experimental process and results.

This study uses the Raytrix R12 Micro light field camera model depicted in Fig. 4, with Table 1 reporting its main open-source parameters. In the experiment, we maximize the utilization of the light field camera sensor by having the aperture of the primary lens equal to the aperture of the microlens array, i.e., adopting the F-number matching principle [26].

Fig. 4. Raytrix R12 Micro light field camera.

Table 1. Parameters of the Raytrix R12 Micro light field camera*

Parameter	Unit	Values
light field camera model	does not have	Raytrix R12 Micro
spatial resolution	pixel	4224×2838
maximum frame rate	fps	5.5
sensor type	does not have	area array CCD
sensor model	does not have	ICX834ALG
sensor size	mm	13.09×8.8
pixel size	μm	3.1×3.1
microlens diameter	pixel	42
number of microlenses	number	98×78

*Source: Raytrix official website https://raytrix.de/

3.1. Microlens center calibration experiment.

The advantage of light field imaging is that a single image can obtain information from multiple perspectives. However, positioning the center of each microlens in an array is particularly important for extracting information from different perspectives. Moreover, acquiring the center coordinates of the microlens array in a light field camera is a prerequisite for achieving all functions in the light field.

The device presented in Fig. 5 allows capturing multiple white plates' original light field images using a light field camera. Then, multiple light field images of white plates are summed and averaged to reduce noise effects. The mean image is used as the ground truth image to calibrate the center of the microlens. In the experiment, the magnification is 3.2 times, the F-number between the microlens and the primary lens is 26, the exposure time is 30 ms, and the distance from the front end face of the primary lens to the white plate is 100 mm. The process of calculating the position of the center of the microlens is as follows: First, we binarize the original white plate image after averaging to obtain an image with multiple microlens circular holes and calculate the center of gravity of each hole. Due to energy accumulation at the center of the microlens, its center of gravity can be considered the center of the microlens. Fig. 6 is a partial enlargement of the original light field image of the white plate, and Fig. 7 is a partial enlargement of the calibration of the center of the microlens, where the red cross is located at the center of the microlens.

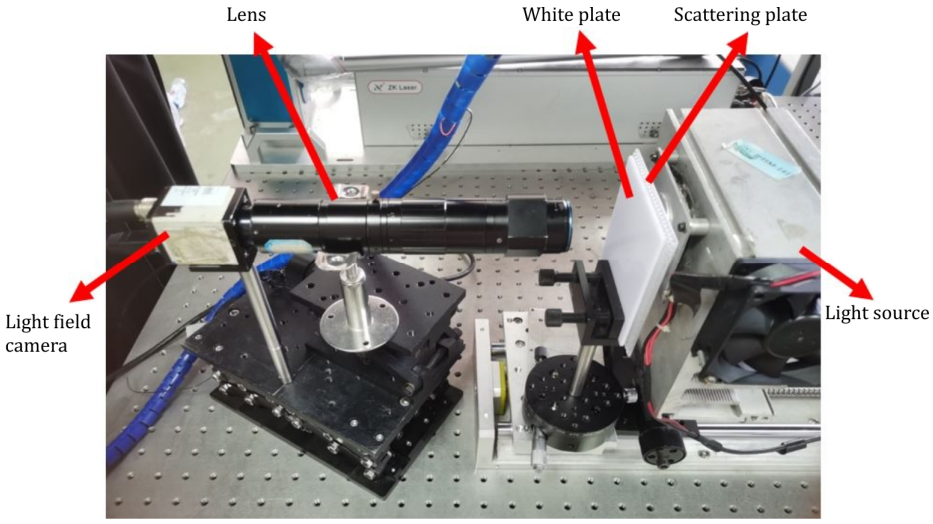

Fig. 5. Experimental setup for calibrating the center of the microlenses.

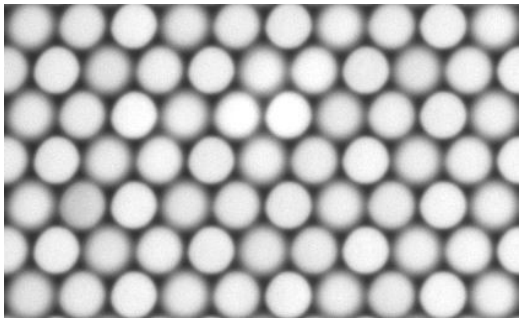

Fig. 6. Partial enlargement of the original light field image of the white plate.

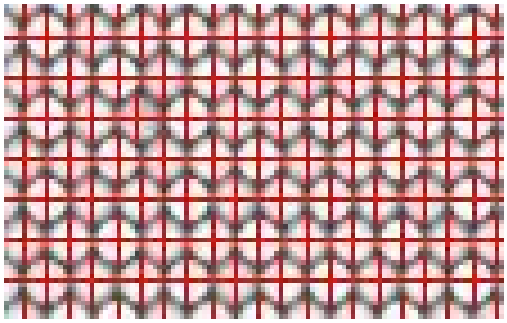

Fig. 7. Partial enlargement of the microlens center calibration.

3.2. Depth calibration experiment.

This article uses a dot calibration plate for depth calibration experiments, with the experimental setup diagram illustrated in Fig. 8. The experimental setup comprises a Raytrix R12 Micro light field camera, a VSZ-0745CO primary lens, an LED backlight, an angle displacement platform, and an electrically operated guide rail. The dot calibration plate has a

diameter of 0.08 mm and a center distance of 0.16 mm between the adjacent dots for depth calibration. During the calibration process, a scattering plate was placed behind the calibration plate to ensure uniform illumination.

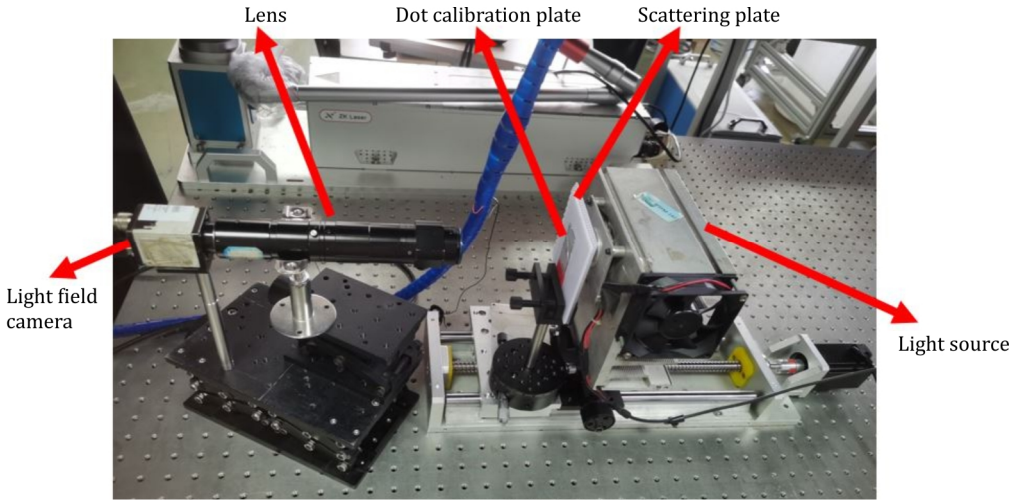

Fig. 8. Experimental setup for depth calibration.

The dot calibration plate was fixed so that the plane of the calibration plate was parallel to the front end face of the primary lens. An electrically operated guide rail was used to change the distance between the front end face of the primary lens and the calibration plate. Five images were acquired with a light field camera every 0.1 mm between 98.1 mm and 102.8 mm. The average of those images was considered the original light field image of the dot calibration plate, which was used for calibration at that position. 48 depth positions were taken, and the exposure time of the light field camera was set to 25 ms, with a magnification of 3.2 times. The F-number of the microlens and the primary lens was 26. Fig. 9 depicts a locally enlarged image of the original light field of the dot calibration plate at different depths.

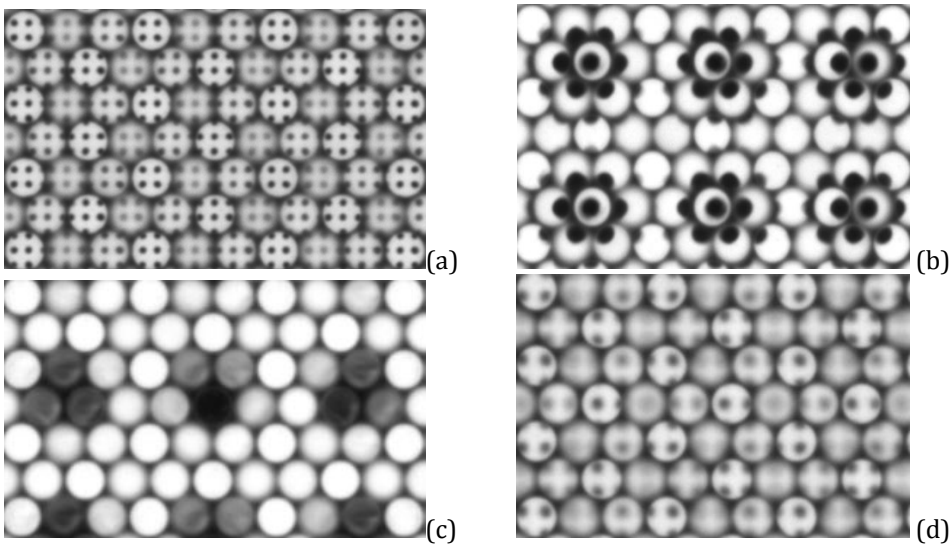

Fig. 9. Partial enlargement of the original light field image of the dot calibration plate: (a) d=98.1 mm,(b) d=100 mm, (c) d=101 mm, (d) d=102.8 mm.

We conducted 500 equally spaced refocusing on the original light field images of the circle calibration plate at each depth position within the range of α_{opt} =0.8÷1.3, resulting in 500 refocused images for each position. Then, the clarity of each refocused image was compared, and the α_{opt} value corresponding to the image with the highest sharpness was considered the optimal refocusing coefficient for that depth *d*. The image sharpness is represented by the image standard deviation δ [27], which represents the degree of dispersion between each pixel and the average grayscale value of the entire image. The related formula is as follows:

$$\delta = \sqrt{\frac{1}{M \times N} \sum_{x=1}^{M} \sum_{y=1}^{N} \left[f(x,y) - \bar{r} \right]}, \tag{4}$$

where *M* and *N* are the number of the image pixels in the *x*, and *y* directions, $f(x,y)$ is the grayscale value of the image at pixel points (x,y), and $\bar{r}$ is the average grayscale value of the entire image. The standard deviation δ reflects the distribution range of pixel values in the image, which can indirectly reflect the clarity of the image. Standard deviation δ can be regarded as the variance of an image. If the variance is small, it means that the pixel value distribution is relatively concentrated, and the image appears blurry; if the variance is large, it means that the pixel value distribution range is wide, and the image looks clearer. So, the maximum sharpness corresponds to the maximum variance determined by Eq.(4). Fig. 10 presents the relationship curve between the refocusing coefficient and sharpness at different depth positions. At the same time, Fig. 11 depicts the relationship curve between the optimal refocusing coefficient $\alpha_{opt}^{\max}$ and its corresponding *d* at each depth position, which is consistent with theoretical analysis.

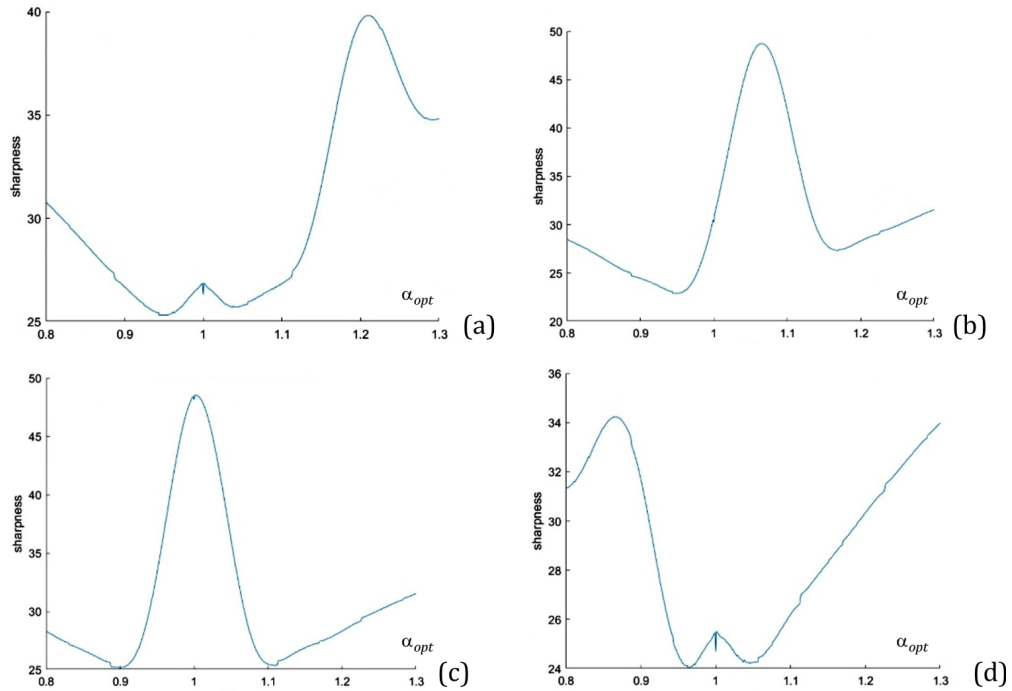

Fig. 10. Relationship between refocusing coefficient and clarity at different depth positions: (a) *d*=98.1 mm, (b) *d*=100 mm, (c) *d*=101 mm, (d) *d*=102.8 mm.

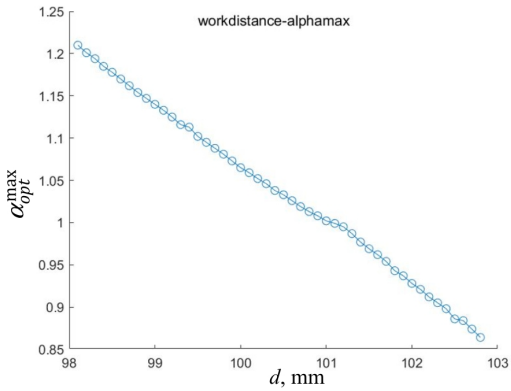

Fig. 11. $d-\alpha_{opt}^{\max}$ calibration curve.

3.3. PSV point light source motion experiment based on light field imaging.

To verify the PSV 3D velocity measurement algorithm based on light field imaging, this paper uses a light field camera to capture 5 μm point light source trajectories moving at speeds of 2 mm/s, 3 mm/s, 4 mm/s, and 5 mm/s on inclined tracks. Long exposure lighting is used during the shooting process, with an exposure time of 100 ms, and the lens parameters are consistent with the calibration process. Fig. 12 presents the experimental setup of a point light source PSV, and Fig. 13 illustrates a locally enlarged view of the streak of a point light source at different speeds.

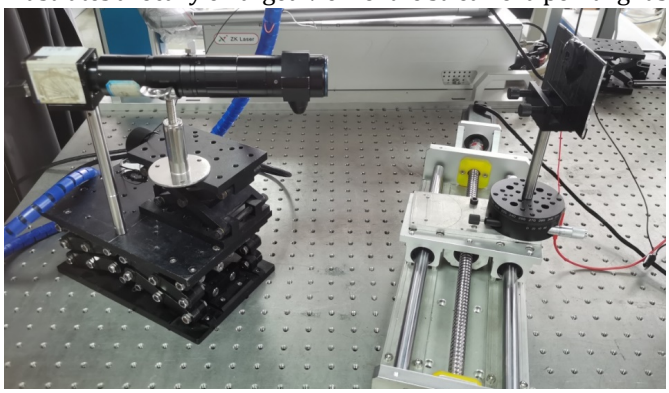

Fig. 12. Experimental setup of the point light source PSV.

After obtaining the original motion streak map of the point light source, all focused images are obtained through image processing. After obtaining the all-focus image, several preprocessing steps are performed, including adaptive multi-threshold segmentation, image dilation, and erosion, removing small targets, refining the skeleton, and removing cross-streak lines. The refocus coefficient at each pixel point, which provides the clearest from the all-focus image, is the optimal refocus coefficient α_{opt}. Then, the previous $d-\alpha_{opt}^{\max}$ calibration data is input to obtain each point's clearest depth data d. Finally, a 3D motion streak map is obtained by indexing the two-dimensional streak data on the all-focus image and combining it with the obtained depth information. Speed information is obtained based on the known exposure time. Fig. 14 presents the all-focus images of the motion streak of a point light source at different speeds. Fig. 15 illustrates a preprocessing image using the motion streak of a point light source at a speed of 4 mm/s as an example. Fig. 16 is a depth map of the motion streak of a point light source at different speeds. In the depth map, different gray levels represent different depth information. The vertical stripes in the map are caused by stray light scattered outward by the point light source during motion. Under the same exposure time, the longer the streak obtained, the more stray light there will be. Of course, this is removed in the image preprocessing stage and will not affect the final processing result. Fig. 17 is a motion streak map of a point light source at a speed of 3 mm/s.

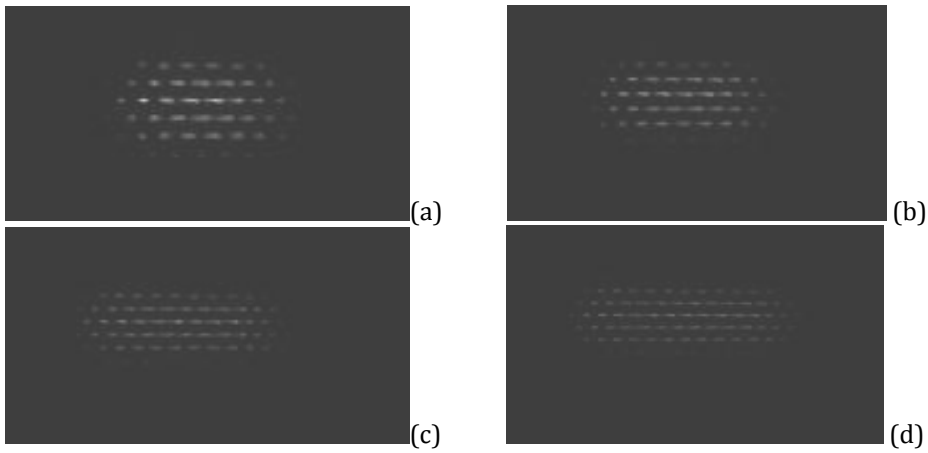

Fig. 13. Partially enlarged view of point light source motion streak at different speeds: (a) 2 mm/s, (b) 3 mm/s,(c) 4 mm/s, (d) 5 mm/s.

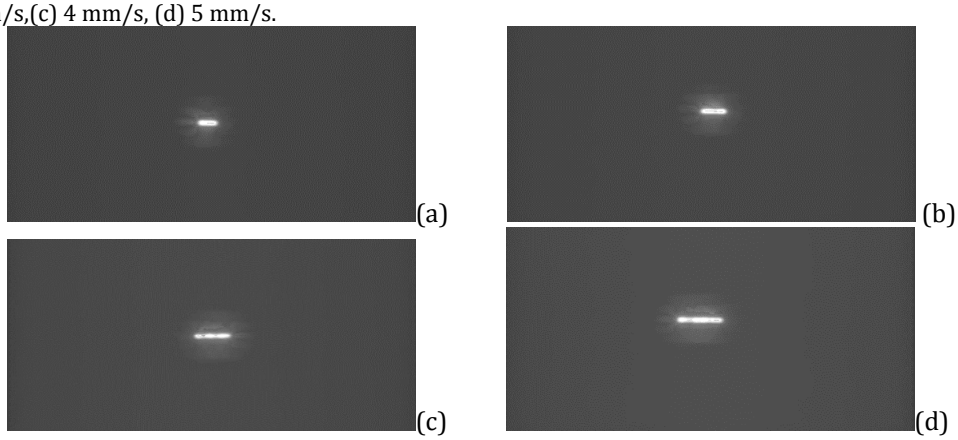

Fig. 14. All-focus images of point light source motion streak at different speeds: (a) 2 mm/s, (b) 3 mm/s, (c) 4 mm/s, (d) 5 mm/s.

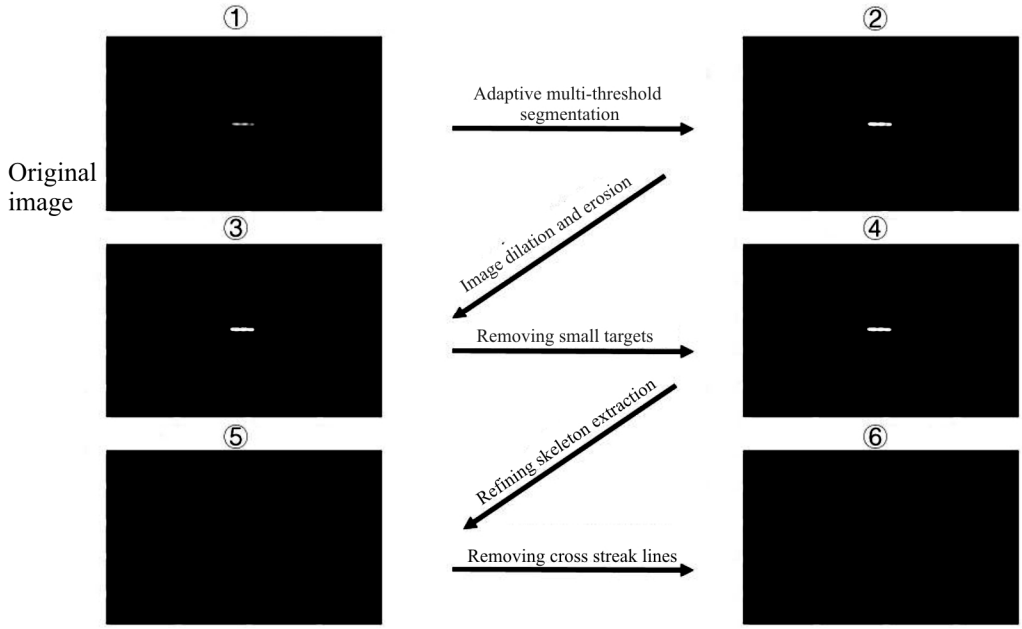

Fig. 15. Preprocessing diagram of point light source motion streak at a speed of 4 mm/s.

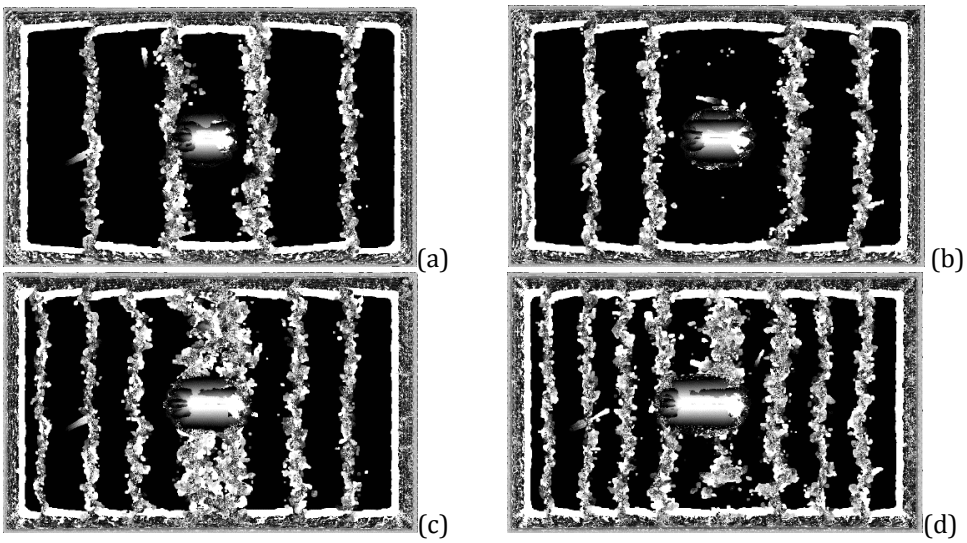

Fig. 16. Depth maps of point light source motion streak at different speeds: (a) 2 mm/s, (b) 3 mm/s, (c) 4 mm/s, (d) 5 mm/s.

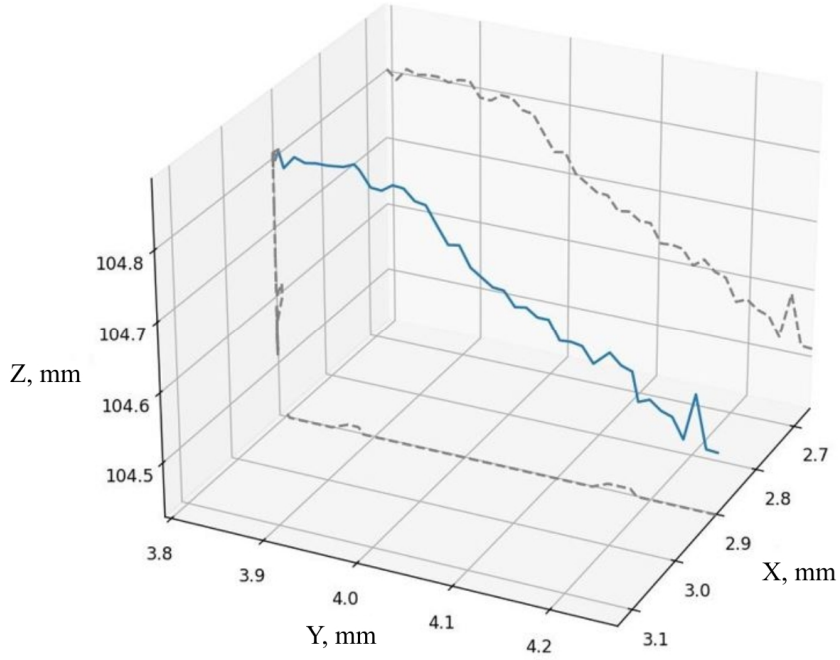

Fig. 17. Motion streaks of point light sources at speed 3 mm/s (the gray dashed lines in the figure are the projection lines).

4. Conclusion

This article employs the principle of light field imaging and elaborates on the refocusing method of light field images. The calibration results obtained are consistent with theoretical analysis. A 3D PSV velocity field measurement method was also introduced based on optical field imaging. Taking the 3D motion of a point light source as an example, the proposed 3D PSV velocity field measurement method based on light field imaging is experimentally validated. The results demonstrated that the proposed 3D velocity field measurement method can be successfully applied utilizing light field PSV. Regarding the velocity direction

ambiguity, the exposure method can be changed to capture motion trajectories of varying lengths to label their motion direction. Future research is needed on this aspect.

Data availability. Data sets generated during the current study are available from the corresponding author upon request.

Acknowledgements. I would like to express my gratitude to EditSprings (https://www.editsprings.cn) for the expert linguistic services provided.

References

1. Liu Huifang, Zhou Wu, Cai Xiaoshu, Zhou Lei, Guo Yan'ang. (2020).Three-dimensional particle tracking velocity measurement technology based on light field imaging. *Journal of Optics*, *40*(1), 0111014.
2. Gershun, A. (1939). The light field. *Journal of Mathematics and Physics*, *18*(1-4), 51-151.
3. Adelson, E. H., & Bergen, J. R. (1991). *The plenoptic function and the elements of early vision* (Vol. 2). Cambridge, MA, USA: Vision and Modeling Group, Media Laboratory, Massachusetts Institute of Technology.
4. McMillan, L., & Bishop, G. (2023). Plenoptic modeling: An image-based rendering system. In *Seminal Graphics Papers: Pushing the Boundaries, Volume 2* (pp. 433-440).
5. Levoy, M., Hanrahan, P. (1996). Light field rendering. *Proceedings of the 23rd annual conference on computer graphics and interactive techniques - SIGGRAPH '96*, August 4-9, 1996, New Orleans, LA, USA. New York: ACM, 31-42.
6. Zhou, Z L. (2012). *Research on light field imaging technology* [Unpublished doctoral dissertation]. University of Science and Technology of China, Hefei.
7. Adelson, E. H., & Wang, J. Y. (1992). Single lens stereo with a plenoptic camera. *IEEE transactions on pattern analysis and machine intelligence*, *14*(2), 99-106.
8. Ng, R. (2006). *Digital light field photography* [Unpublished doctoral dissertation]. Stanford University.
9. Lumsdaine, A., & Georgiev, T. (2009, April). The focused plenoptic camera. In *2009 IEEE international conference on computational photography (ICCP)* (pp. 1-8). IEEE.
10. Alarcon, R., Allen, J., Thurow, B. S., & Moss, A. (2020). Development of a high-speed plenoptic imaging system and its application to marine biology PIV. *Measurement Science and Technology*, *31*(5), 054005.
11. Broxton, M., Grosenick, L., Yang, S., Cohen, N., Andalman, A., Deisseroth, K., & Levoy, M. (2013). Wave optics theory and 3-D deconvolution for the light field microscope. *Optics Express*, *21*(21), 25418-25439.
12. Lynch, K., Fahringer, T., & Thurow, B. (2012). Three-dimensional particle image velocimetry using a plenoptic camera. In *50th AIAA aerospace sciences meeting including the new horizons forum and aerospace exposition* (p. 1056).
13. Fahringer, T. W., Lynch, K. P., & Thurow, B. S. (2015). Volumetric particle image velocimetry with a single plenoptic camera. *Measurement Science and Technology*, *26*(11), 115201.
14. Fahringer, T., & Thurow, B. (2012, June). Tomographic reconstruction of a 3-D flow field using a plenoptic camera. In *42nd AIAA fluid dynamics conference and exhibit.* (p. 2826).
15. Bolton, J. T., Thurow, B. S., Alvi, F. S., & Arora, N. (2017). Single camera 3D measurement of a shock wave-turbulent boundary layer interaction. In *55th AIAA Aerospace Sciences Meeting* (p. 0985).
16. Thurow, B., Tan, Z., Tiwari, B., & Raghav, V. (2019, November). Technique for Characterization of 3D Unsteady Fluid-Structure Interactions via a Single Plenoptic Camera. In *APS Division of Fluid Dynamics Meeting Abstracts* (pp. P11-008).
17. Kelly, D., Clifford, C., & Thurow, B. (2020). 2D and 3D Temperature Measurements with a Multi-band Plenoptic Camera. In *APS Division of Fluid Dynamics Meeting Abstracts* (pp. T07-009).
18. Jones, C., Bolton, J., Clifford, C., Thurow, B., Arora, N., & Alvi, F. (2020). Single-camera three-dimensional velocity measurement of a fin-generated shock-wave/boundary-layer interaction. *AIAA Journal*, *58*(10), 4438-4450.
19. Willneff, J., & Gruen, A. (2002). A new spatio-temporal matching algorithm for 3D-particle tracking velocimetry. In *9th International symposium on transport phenomena and dynamics of rotating machinery*. ETH Zurich, Institute of Geodesy and Photogrammetry.
20. Pereira, F., Stüer, H., Graff, E. C., & Gharib, M. (2006). Two-frame 3D particle tracking. *Measurement Science and Technology*, *17*(7), 1680.
21. Hoyer, K., Holzner, M., Lüthi, B., Guala, M., Liberzon, A., & Kinzelbach, W. (2005). 3D scanning particle tracking velocimetry. *Experiments in Fluids*, *39*, 923-934.
22. Satake, S. I., Kunugi, T., Sato, K., Ito, T., Kanamori, H., & Taniguchi, J. (2006). Measurements of 3D flow in a micro-pipe via micro digital holographic particle tracking velocimetry. *Measurement Science and Technology*, *17*(7), 1647.

23. Dimotakis, P. E., Debussy, F. D., & Koochesfahani, M. M. (1981). Particle streak velocity field measurements in a two-dimensional mixing layer. *Physics of Fluids*, *24*(6), 995-999.
24. Adrian, R. J. (1984). Scattering particle characteristics and their effect on pulsed laser measurements of fluid flow: speckle velocimetry vs particle image velocimetry. *Applied Optics*, *23*(11), 1690-1691.
25. Adamczyk, A. A., & Rimai, L. (1988). 2-Dimensional particle tracking velocimetry (PTV): technique and image processing algorithms. *Experiments in fluids*, *6*(6), 373-380.
26. Perwass, C., & Wietzke, L. (2012, February). Single lens 3D-camera with extended depth-of-field. In *Human vision and electronic imaging XVII* (Vol. 8291, pp. 45-59). SPIE.
27. Fang Xiaoyan. (2017). Image quality evaluation algorithm based on clarity detection and human-computer interaction. *Foreign Electronic Measurement Technology*. *36* (4), 32-35.

Miao Yang. (2024). A Three-Dimensional Flow Field Measurement Method Based on Light Field Particle Streak Velocimetry**.** *Ukrainian Journal of Physical Optics*, *25*(4), 04038 – 04050. doi: 10.3116/16091833/Ukr.J.Phys.Opt.2024.04038

Анотація*. З використанням камер світлового поля можна отримувати просторову 3D інформацію про об'єкти, з єдиного зображення, що демонструє те, що технологія зйомки не потребує організації складного проходження світла. Завдяки цій можливості камери світлого поля нещодавно привернули увагу в різних галузях. Крім того, трекове вимірювання швидкості частинок (PSV) є безконтактним методом вимірювання поля потоку на основі зображень, який широко використовується в оптичних технологіях і технологіях обробки зображень. Він має очевидні переваги у вимірюванні полів високошвидкісного потоку. Таким чином, ця стаття поєднує технологію зображення світлового поля з технологією PSV і представляє нову 3D систему вимірювання швидкості, яка використовує переваги обох технологій для вимірювання полів потоку з вузькими вікнами, високою швидкістю потоку та складним для організації вимірювальним обладнанням. Розроблена система формує тривимірний метод вимірювання поля потоку на основі світлового поля PSV, який є унікальним, оскільки жодне відповідне дослідження вимірювання 3D швидкості PSV не використовує зображення світлового поля. Зокрема, за допомогою камери світлового поля, була зафіксований трек руху точкового джерела світла розміром5 мкм, що рухається з різними швидкостями, а його тривимірне поле швидкості було перевірено та розраховано за допомогою обчислювальної системи. Результати продемонстрували, що метод вимірювання 3D поля потоку на основі PSV світлового поля може успішно вимірювати 3D поля потоку.*

Ключові слова*: візуалізація світлового поля, 3D вимірювання, трекове вимірювання швидкості частинок*